PAPER

Electron beam-plasma interaction and electron-acoustic solitary waves in a plasma with suprathermal electrons

To cite this article: A Danehkar 2018 *Plasma Phys. Control. Fusion* **60** 065010

View the article online for updates and enhancements.

Electron beam-plasma interaction and electron-acoustic solitary waves in a plasma with suprathermal electrons

A Danehkar[1]

Centre for Plasma Physics, Queen's University Belfast, Belfast BT7 1NN, United Kingdom
Department of Physics and Astronomy, Macquarie University, Sydney, NSW 2109, Australia

E-mail: ashkbiz.danehkar@cfa.harvard.edu

Abstract

Suprathermal electrons and inertial drifting electrons, so called electron beam, are crucial to the nonlinear dynamics of electrostatic solitary waves observed in several astrophysical plasmas. In this paper, the propagation of electron-acoustic solitary waves (EAWs) is investigated in a collisionless, unmagnetized plasma consisting of cool inertial background electrons, hot suprathermal electrons (modeled by a κ-type distribution), and stationary ions. The plasma is penetrated by a cool electron beam component. A linear dispersion relation is derived to describe small-amplitude wave structures that shows a weak dependence of the phase speed on the electron beam velocity and density. A (Sagdeev-type) pseudopotential approach is employed to obtain the existence domain of large-amplitude solitary waves, and investigate how their nonlinear structures depend on the kinematic and physical properties of the electron beam and the suprathermality (described by κ) of the hot electrons. The results indicate that the electron beam can largely alter the EAWs, but can only produce negative polarity solitary waves in this model. While the electron beam co-propagates with the solitary waves, the soliton existence domain (Mach number range) becomes narrower (nearly down to nil) with increasing the beam speed and the beam-to-hot electron temperature ratio, and decreasing the beam-to-cool electron density ratio in high suprathermality (low κ). It is found that the electric potential amplitude largely declines with increasing the beam speed and the beam-to-cool electron density ratio for co-propagating solitary waves, but is slightly decreased by raising the beam-to-hot electron temperature ratio.

Keywords: electron-acoustic waves, electron beams, nonlinear processes, plasma solitons

(Some figures may appear in colour only in the online journal)

1. Introduction

Nonlinear electron-acoustic solitary waves (EAWs) are typically produced in a plasma composed of two electron temperature populations, so called *cool* and *hot* electrons [1–4], which have been observed in many space plasmas [5–10]. In such a plasma, the wave restoring force is provided by the thermal pressure of the hot electrons, whereas the cool electrons provide the inertia to support electron-acoustic oscillations. The phase speed of the EAWs is typically intermediate between the cool and hot electron thermal velocities. It has been pointed out that the EAWs only propagate within a restricted range of the physical conditions, i.e., the hot-to-cool electron number density ratio between 1/4 and 4, and the hot-to-cool electron temperature ratio is greater than 10 [3, 11, 12]. As the EAW frequency is much higher than the ion plasma frequency, the ions may not largely affect the EAWs, and they usually play the role of a neutralizing background in the plasma.

The observations of the upper layer of the Earth's magnetosphere revealed the injection of magnetic field-aligned drifting electrons from solar winds, the so called *electron beam*, into two different (cool and hot) electron populations [13–20], which may excite the EAWs and modify their existence conditions and nonlinear wave structures. It has been found that the auroral broadband electrostatic noise (BEN) emissions observed in the Earth's magnetosphere strongly correlate with the magnetic field-aligned electron beams [17]. In particular, the high time-resolution GEOTAIL observations of the Earth's auroral region showed that the BEN consists a series of nonlinear localized electrostatic solitary waves, which are associated with the nonlinear dynamics of the electron beam instability [18]. The generation of electrostatic solitary waves was also reported in the polar cap boundary layer (PCBL) region, which are locally involved electron beams [20]. More recently, the Magnetospheric Multiscale (MMS) Mission observations of the Earth's magnetosphere revealed electrostatic solitary waves in the magnetosheath and magnetopause, likely supported by a *cool* ($\sim$1–20 eV) field-aligned drifting electron component [21, 22]. The effects of electron beams have been investigated in EAWs [23–33]. Electron beams allow the propagation of EAWs with velocity related to the beam speed, whereas their amplitude and width depend on the beam physical properties [23, 24]. It has been found that a hole (hump) in the cool (hot) electron number density, which is not present without electron beam, allows the propagation of positively polarized electrostatic solitary waves [23, 25–27].

A population of energetic *hot* ($\sim$1–20 keV at Earth's bow shock [34]) electrons with *suprathermal* distributions has been reported in various space plasmas [35]. This population was found to have a suprathermal (or non-thermal) tail on its velocity distribution function, and its kinetic energy is much higher than the thermal energy of the background cool inertial electrons. It has been shown that these suprathermal hot electrons are well described by a family of κ-distribution functions [36]. The deviation from a Maxwellian distribution is described by the spectral index κ, i.e., low values of κ are associated with a significant suprathermality, whereas a Maxwellian distribution is recovered in the limit $\kappa \to \infty$ [37–39]. Suprathermal (and non-thermal) electrons have recently been incorporated into theoretical models of EAWs [40–49]. It has been found that higher deviations from a Maxwellian raise negative polarity EAWs [40–43], though the soliton existence regions become narrower [41, 42]. Moreover, electron-acoustic shock structures were found to become narrower and steeper in higher suprathermality [44].

Recently, a number of papers have been devoted to the effects of both electron beams and suprathermal electrons on EAWs [30, 31, 49–51]. However, the positive polarity signature, which was previously found for EAWs [23], was not reproduced using κ-distributed electrons [30], which might be due to the chosen parameter range. Previously, a plasma with suprathermal electrons, inertial warm electron beam, inertial cool electron and inertial (mobile) ions were found to produce

both positive and negative electrostatic potentials [31]. To have positively polarized electrostatic waves, the inertia of the warm electrons, not the beam velocity, seems to be important [31]. However, it requires a rather high density of cool electrons [31–33], which does not seem to correspond to available observations [52, 53]. Alternatively, mobile ions [54–56] or inertial positrons (or electron holes) [57, 58] can provide the inertia for the propagation of positive polarity electrostatic waves with suprathermal electrons in the slow (ion) or fast (positron) acoustic modes, respectively.

In this paper, we aim to investigate the effects of an electron beam component, together with suprathermal κ-distributed electrons, on the existence conditions and properties of the EAWs. A theoretical two-fluid model is presented in section 2. In section 3, we derive a linear dispersion relation for the small-amplitude EAWs. In section 4, the Sagdeev pseudopotential method is employed to obtain the nonlinear solution of the large-amplitude EAWs. The occurrence of EAWs is investigated in section 5. In section 6, we investigate the electron beam effects on the characteristics of EAWs. Our conclusions are given in section 7.

2. Theoretical two-fluid model

We consider a four-component collisionless, unmagnetized plasma consisting of cool inertial background electrons (at temperature $T_c \neq 0$), cool inertial electron beam (at temperature $T_b \neq 0$), hot inertialess suprathermal electrons modeled by a κ-distribution (at temperature $T_h \gg T_b, T_c$), and uniformly distributed stationary ions.

The fluid model is governed by the following one-dimensional equations:

$$\frac{\partial n_j}{\partial t} + \frac{\partial (n_j u_j)}{\partial x} = 0, \tag{1}$$

$$\frac{\partial u_j}{\partial t} + u_j \frac{\partial u_j}{\partial x} = \frac{e}{m_e} \frac{\partial \phi}{\partial x} - \frac{1}{m_e n_j} \frac{\partial p_j}{\partial x}, \tag{2}$$

$$\frac{\partial p_j}{\partial t} + u_j \frac{\partial p_j}{\partial x} + \gamma p_j \frac{\partial u_j}{\partial x} = 0, \tag{3}$$

$$n_h(\phi) = n_{h,0} \left[1 - \frac{e\phi}{k_B T_h (\kappa - \frac{3}{2})} \right]^{-\kappa + 1/2}, \tag{4}$$

$$Z n_{i,0} = n_{c,0} + n_{b,0} + n_{h,0}, \tag{5}$$

$$\frac{\partial^2 \phi}{\partial x^2} = -\frac{e}{\varepsilon_0} (Z n_{i,0} - n_c - n_b - n_h), \tag{6}$$

where n_j, u_j and p_j are, respectively, the number density, the velocity and the pressure of the cool background electrons (denoted by index $j = c$) and the electron beam (denoted by index $j = b$), $n_{h,0}$ and T_h are, respectively, the equilibrium number density and the temperature of the hot electrons modeled by the κ-distribution equation (4) [37–39], the spectral index κ measures the deviation from a Maxwellian distribution ($\kappa > 3/2$), $n_{i,0}$ the undisturbed ion density, Z the number of ions, ϕ the electrostatic wave potential, e the

elementary charge, m_e the electron mass, ε_0 the permittivity constant, k_B the Boltzmann constant, and $\gamma = (f + 2)/f$ denotes the specific heat ratio for f degrees of freedom. For the adiabatic (cool and beam) electrons in 1D ($f = 1$), we get $\gamma = 3$. The ions are assumed to be stationary, i.e., $n_i = n_{i,0} = $ const. at all times. As the plasma is quasi-neutral at equilibrium, we have equation (5), where $n_{c,0}$ and $n_{b,0}$ are the equilibrium number density of the cool background electrons and the electron beam, respectively. All four components are coupled via the Poisson's equation (6).

Normalizing equations (1)–(6) by appropriate quantities, we obtain a dimensionless set of fluid equations as follows:

$$\frac{\partial n_j}{\partial t} + \frac{\partial (n_j u_j)}{\partial x} = 0, \tag{7}$$

$$\frac{\partial u_j}{\partial t} + u_j \frac{\partial u_j}{\partial x} = \frac{\partial \phi}{\partial x} - \frac{\theta_{j,h}}{n_j} \frac{\partial p_j}{\partial x}, \tag{8}$$

$$\frac{\partial p_j}{\partial t} + u_j \frac{\partial p_j}{\partial x} + 3 p_j \frac{\partial u_j}{\partial x} = 0, \tag{9}$$

$$\frac{\partial^2 \phi}{\partial x^2} = -(1 + \rho_{h,c} + \rho_{b,c}) + n_c$$
$$+ \rho_{b,c} n_b + \rho_{h,c} \left(1 - \frac{\phi}{\kappa - \frac{3}{2}}\right)^{-\kappa + 1/2}, \tag{10}$$

where the density variables n_c and n_b are, respectively, normalized by $n_{c,0}$ and $n_{b,0}$, the velocities u_c and u_b scaled by the hot electron thermal speed $c_{th} = (k_B T_h/m_e)^{1/2}$, the wave potential ϕ scaled by $k_B T_h/e$, and time and space scaled by the plasma period $\omega_{pc}^{-1} = (n_{c,0}e^2/\varepsilon_0 m_e)^{-1/2}$ and the characteristic length $\lambda_0 = (\varepsilon_0 k_B T_h/n_{c,0}e^2)^{1/2}$, respectively. The normalized beam speed is defined as $V_b = u_{b,0}/c_{th}$, where $u_{b,0}$ is the beam velocity at equilibrium. The hot-to-cool electron number density ratio, $\rho_{h,c}$, and the beam-to-cool electron number density ratio, $\rho_{b,c}$, are respectively defined as

$$\rho_{h,c} = n_{h,0}/n_{c,0}, \qquad \rho_{b,c} = n_{b,0}/n_{c,0},$$

which imply $Z n_{i,0}/n_{c,0} = 1 + \rho_{h,c} + \rho_{b,c}$.

Landau damping is minimized if $0.2 \lesssim n_{c,0}/(n_{c,0} + n_{h,0}) \lesssim 0.8$ [3, 11, 12]. We consider the region $0.25 \leqslant \rho_{h,c} \leqslant 4$ in which the linear waves are not strongly damped. The cool-to-hot electron temperature ratio, $\theta_{c,h}$, and the beam-to-hot electron temperature ratio, $\theta_{b,h}$, are defined respectively as

$$\theta_{c,h} = T_c/T_h, \qquad \theta_{b,h} = T_b/T_h.$$

The linear waves survive Landau damping if $T_h/T_c \gg 10$ [3, 11, 12], so we consider the region $\theta_{c,h} \ll 0.1$ where the waves are not strongly damped. Similarly, EAWs excited by the electron beam are weakly damped when the hot to beam electron temperature ratio becomes more than 10. We notice that the observations of the BEN in the auroral zone indicated that the presence of magnetic field-aligned electron beams with $T_b \sim 1$ eV, while hot electron population with $T_h \sim 500$ eV [59], or $T_b \sim 50$ eV and $T_h \sim 200$–990 eV [17]. Moreover, the observations of the PCBL region

pointed $T_b \sim 100$ eV and $T_h \sim 25$ keV [20]. Recently, the MMS observations of the magnetosphere plasma reported field-aligned drifting electrons with $T_b \sim 1$–20 eV [21, 22] along with hot electrons having $T_h \sim 1$ keV [21]. Hence, we can assume $\theta_{b,h} \ll 0.1$.

To preserve the excitation of electrostatic waves, there should be no wave magnetic effects and no current from Ampère's law [60], i.e. $j_{b,0} = n_{b,0}u_{b,0} \simeq 0$. Thus, the electron beam speed V_b and the beam-to-cool electron number density ratio $\rho_{b,c}$ should satisfy the trivially current condition $\rho_{b,c}V_b \ll 1$ [55], in addition to the weakly damped condition $\theta_{b,h} \ll 0.1$ for the beam-to-hot electron temperature ratio, in order to maintain the excitation of EAWs as the electron beam penetrates into the plasma.

3. Linear dispersion relation

To study linear small-amplitude wave solutions of the fluid model, we obtain linearized forms of equations (7)–(10). We apply a small deviation from the equilibrium state, which produces the derivatives of the first order amplitudes, and keep the expansion up to first order. The linear dispersion relation for EAWs is then as follows:

$$1 + \frac{\rho_{h,c}}{k^2}\left(\frac{\kappa - \frac{1}{2}}{\kappa - \frac{3}{2}}\right) = \frac{1}{\omega^2 - 3\theta_{c,h}k^2}$$
$$+ \frac{\rho_{b,c}}{(\omega - kV_b)^2 - 3\theta_{b,h}k^2}, \tag{11}$$

where $\sqrt{3\theta_{c,h}}$ and $\sqrt{3\theta_{b,h}}$ are basically the (normalized) thermal velocities of the cool electrons and the electron beam, respectively.

Equation (11) indicates that the phase speed (ω/k) increases with raising the cool-to-hot electron temperature ratio $\theta_{c,h} = T_c/T_h$, which is in agreement with [42]. Although the frequency $\omega(k)$ (also the phase speed) increases with raising the beam-to-hot electron temperature ratio $\theta_{b,h} = T_b/T_h$, this linear effect is negligible due to small values of the beam-to-cool electron number density ratio $\rho_{b,c}$. In the limit $\rho_{b,c} \to 0$ (in the absence of the electron beam), equation (11) recovers precisely equation (14) in [42].

Figure 1 shows the dispersion curve (11) of the electron-acoustic mode in the cold limit ($T_c = T_b = 0$). It can be seen how varying the electron beam parameters V_b and $\rho_{b,c}$ affect the dispersion curve. The phase speed increases weakly with an increase in V_b and $\rho_{b,c}$. Additionally, an increase in the number density of suprathermal hot electrons or/and the suprathermality (decreasing κ) also decreases the phase speed (see figure 1 in [42]).

Following [12], the wave avoids being strongly damped if its phase velocity is between the cool electron and hot electron thermal speed $c_{tc} \ll \omega/k \ll c_{th}$ (or the normalized region here $\sqrt{\theta_{c,h}} \ll \omega/k \ll 1$). Moreover, the wave is weakly damped for $0.2 \lesssim k\lambda_{Dc} \lesssim 0.6$, so this region could be of interest only. Here, $c_{tc} = (k_B T_c/m_e)^{1/2}$ is the cool electron thermal speed, and $\lambda_{Dc} = (\varepsilon_0 k_B T_c/n_{c,0}e^2)^{1/2}$ is the cool
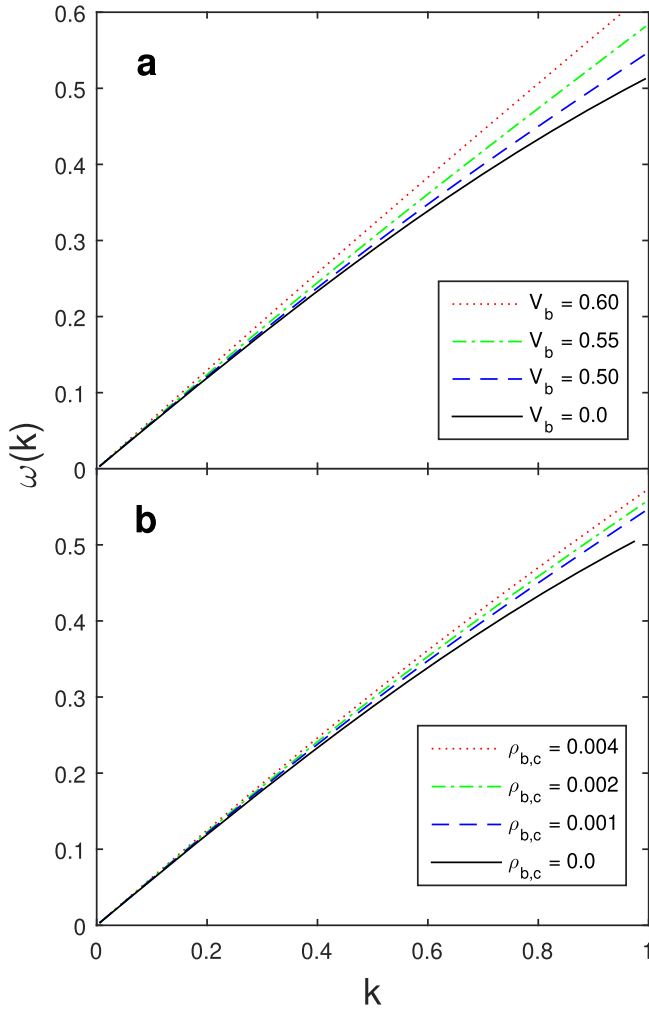
Figure 1. (a) Variation of the dispersion curve for different values of the normalized beam speed V_b is depicted. Curves from bottom to top: $V_b = 0$ (solid), 0.5 (dashed), 0.55 (dotted–dashed), and 0.6 (dotted curve). Here, $\rho_{b,c} = 0.001$. (b) Variation of the dispersion curve for different values of the beam-to-cool electron number density ratio $\rho_{b,c}$. Curves from bottom to top: $\rho_{b,c} = 0.0$ (solid), 0.001 (dashed), 0.002 (dotted–dashed curve), and 0.004 (dotted curve). Here, $V_b = 0.5$. For both panels, we have taken: $\rho_{h,c} = 1$, $\kappa = 3$, and $\theta_{c,h} = \theta_{b,h} = 0$.

electron Debye length. As seen in figure 1, the phase speed of the linear wave is inside the weakly damped region ($0 < \omega/k < 1$, while $T_c = T_b = 0$). The physical conditions for minimizing weakly Landau damping ($0.25 \leqslant \rho_{h,c} \leqslant 4$, $\theta_{c,h} \ll 0.1$) may also prevent the phase velocity of the waves being strongly Landau damped by either of the cool or hot electrons.

4. Nonlinear pseudopotential approach

To obtain nonlinear large-amplitude wave solutions of the fluid model, it is convenient to consider a stationary frame moving with a constant normalized velocity M, so called the Mach number. This implies the transformation $\xi = x - Mt$ that replaces the space and time derivatives

with $\partial/\partial x = \mathrm{d}/\mathrm{d}\xi$ and $\partial/\partial t = -M\mathrm{d}/\mathrm{d}\xi$, respectively. Equations (7)–(10) in the corresponding reference frame take the following form:

$$-M\frac{\mathrm{d}n_c}{\mathrm{d}\xi} + \frac{\mathrm{d}(n_c u_c)}{\mathrm{d}\xi} = 0, \tag{12}$$

$$-M\frac{\mathrm{d}u_c}{\mathrm{d}\xi} + u_c\frac{\mathrm{d}u_c}{\mathrm{d}\xi} = \frac{\mathrm{d}\phi}{\mathrm{d}\xi} - \frac{\theta_{c,h}}{n_c}\frac{\mathrm{d}p_c}{\mathrm{d}\xi}, \tag{13}$$

$$-M\frac{\mathrm{d}p_c}{\mathrm{d}\xi} + u_c\frac{\mathrm{d}p_c}{\mathrm{d}\xi} + 3p_c\frac{\mathrm{d}u_c}{\mathrm{d}\xi} = 0, \tag{14}$$

$$-M\frac{\mathrm{d}n_b}{\mathrm{d}\xi} + \frac{\mathrm{d}(n_b u_b)}{\mathrm{d}\xi} = 0, \tag{15}$$

$$-M\frac{\mathrm{d}u_b}{\mathrm{d}\xi} + u_b\frac{\mathrm{d}u_b}{\mathrm{d}\xi} = \frac{\mathrm{d}\phi}{\mathrm{d}\xi} - \frac{\theta_{b,h}}{n_b}\frac{\mathrm{d}p_b}{\mathrm{d}\xi}, \tag{16}$$

$$-M\frac{\mathrm{d}p_b}{\mathrm{d}\xi} + u_b\frac{\mathrm{d}p_b}{\mathrm{d}\xi} + 3p_b\frac{\mathrm{d}u_b}{\mathrm{d}\xi} = 0, \tag{17}$$

$$\frac{\mathrm{d}^2\phi}{\mathrm{d}\xi^2} = -(1 + \rho_{h,c} + \rho_{b,c}) + n_c + \rho_{b,c}n_b$$
$$+ \rho_{h,c}\left(1 - \frac{\phi}{\kappa - \frac{3}{2}}\right)^{-\kappa+1/2}. \tag{18}$$

It is assume that the equilibrium state is reached at infinities ($\xi \to \pm\infty$). We then integrate the above fluid equations, apply the boundary conditions $n_c = 1$, $p_c = 1$, $u_c = 0$, $n_b = 1$, $p_b = 1$, $u_b = V_b$ and $\phi = 0$ at infinities, and derive

$$u_c = M[1 - (1/n_c)], \tag{19}$$

$$u_c = M - (M^2 + 2\phi - 3n_c^2\theta_{c,h} + 3\theta_{c,h})^{1/2}, \tag{20}$$

$$u_b = M[1 - (1/n_b)(1 - V_b/M)], \tag{21}$$

$$u_b = M - [(M - V_b)^2 + 2\phi - 3n_b^2\theta_{b,h} + 3\theta_{b,h}]^{1/2}, \tag{22}$$

$$p_c = n_c^3, \qquad p_b = n_b^3. \tag{23}$$

Combining equations (19)–(23) and solving them lead to the following solutions for the cool electron density, n_c, and the electron beam density, n_b, respectively:

$$n_c = \frac{1}{2\sqrt{3\theta_{c,h}}}[2\phi + (M + \sqrt{3\theta_{c,h}})^2]^{1/2}$$
$$\pm \frac{1}{2\sqrt{3\theta_{c,h}}}[2\phi + (M - \sqrt{3\theta_{c,h}})^2]^{1/2}, \tag{24}$$

$$n_b = \frac{1}{2\sqrt{3\theta_{b,h}}}[2\phi + (M - V_b + \sqrt{3\theta_{b,h}})^2]^{1/2}$$
$$\pm \frac{1}{2\sqrt{3\theta_{b,h}}}[2\phi + (M - V_b - \sqrt{3\theta_{b,h}})^2]^{1/2}. \tag{25}$$

Equation (24) is exactly the same as equation (29) in [42]. Taking the boundary conditions $n_c = n_b = 1$ at $\phi = 0$, the negative sign must be used in equations (24) and (25). Furthermore, the cool electrons and the electron beam are supersonic at

$M > \sqrt{3\theta_{c,h}}$ and $M > V_b + \sqrt{3\theta_{b,h}}$, while the hot electrons are subsonic at $M < 1$. Considering the reality conditions of the density variables, the limits on the electrostatic potential value become $\phi > \phi_{\lim(-)} = -\frac{1}{2}(M - \sqrt{3\theta_{c,h}})^2$ for $V_b \leqslant 0$ (counter-propagation case), and $-\frac{1}{2}(M - V_b - \sqrt{3\theta_{b,h}})^2$ for $V_b > 0$ (co-propagation case), which are associated with negatively polarized electrostatic solitary wave structures.

Substituting equations (24)–(25) into the Poisson's equation, multiplying the resulting equation by $d\phi/d\xi$, integrating and taking into account the conditions at infinities $(d\phi/d\xi \to 0)$ yield a pseudo-energy balance equation

$$\frac{1}{2}\left(\frac{d\phi}{d\xi}\right)^2 + \Psi(\phi) = 0, \tag{26}$$

where the Sagdeev pseudopotential $\Psi(\phi)$ is given by

$$\begin{aligned}
\Psi(\phi) = &\ \rho_{h,c}\left[1 - \left(1 + \frac{\phi}{-\kappa + \frac{3}{2}}\right)^{-\kappa + 3/2}\right] \\
&+ (1 + \rho_{h,c} + \rho_{b,c})\phi \\
&+ \frac{1}{6\sqrt{3\theta_{c,h}}}[(M + \sqrt{3\theta_{c,h}})^3 - (M - \sqrt{3\theta_{c,h}})^3 \\
&- (2\phi + [M + \sqrt{3\theta_{c,h}}]^2)^{3/2} \\
&+ (2\phi + [M - \sqrt{3\theta_{c,h}}]^2)^{3/2}] \\
&+ \frac{\rho_{b,c}}{6\sqrt{3\theta_{b,h}}}[(M - V_b + \sqrt{3\theta_{b,h}})^3 \\
&- (M - V_b - \sqrt{3\theta_{b,h}})^3 \\
&- (2\phi + [M - V_b + \sqrt{3\theta_{b,h}}]^2)^{3/2} \\
&+ (2\phi + [M - V_b - \sqrt{3\theta_{b,h}}]^2)^{3/2}].
\end{aligned} \tag{27}$$

In the absence of the electron beam ($\rho_{b,c} \to 0$), we precisely recover equation (33) in [42].

5. Existence conditions for electron-acoustic solitons

To maintain solitary waves, the origin at $\phi = 0$ must be a root and a local maximum of Ψ in equation (27), so $\Psi(\phi) = 0$, $\Psi'(\phi) = 0$ and $\Psi''(\phi) < 0$ at $\phi = 0$, where primes denote derivatives with respect to ϕ. As the first two constraints are satisfied, the condition for the lower limit becomes $F_1(M) = -\Psi''(\phi)|_{\phi=0} > 0$. This yields the following equation for the minimum value for the Mach number M:

$$\begin{aligned}
F_1(M) = &\ \frac{\rho_{h,c}(\kappa - \frac{1}{2})}{\kappa - \frac{3}{2}} - \frac{1}{M^2 - 3\theta_{c,h}} \\
&- \frac{\rho_{b,c}}{(M - V_b)^2 - 3\theta_{b,h}}.
\end{aligned} \tag{28}$$

Equation (28) constrains the lower limit for the Mach number, M_1 (κ, $\rho_{h,c}$, $\theta_{c,h}$, $\rho_{b,c}$, $\theta_{b,h}$, V_b).

An upper limit for M is obtained when the density profile reaches the complex value at $\phi_{\lim(-)} = -\frac{1}{2}(M - \sqrt{3\theta_{c,h}})^2$ for $V_b \leqslant 0$ (counter-propagation case) and $\phi_{\lim(-)} = -\frac{1}{2}(M - V_b - \sqrt{3\theta_{b,h}})^2$ for $V_b > 0$ (co-propagation case). Thus, the largest soliton amplitude satisfies $F_2(M) = \Psi(\phi)|_{\phi=\phi_{\lim(-)}} > 0$. This yields the following equation for the upper limit in M in the case of *counter-propagating* ($V_b \leqslant 0$),

$$\begin{aligned}
F_2(M) = &\ -\frac{1}{2}(1 + \rho_{h,c} + \rho_{b,c})(M - \sqrt{3\theta_{c,h}})^2 \\
&- \frac{4}{3}M^{3/2}(3\theta_{c,h})^{1/4} \\
&+ \rho_{h,c}\left[1 - \left(1 + \frac{[M - \sqrt{3\theta_{c,h}}]^2}{2\kappa - 3}\right)^{-\kappa + 3/2}\right] \\
&+ M^2 + \theta_{c,h} + \rho_{b,c}(M - V_b)^2 + \rho_{b,c}\theta_{b,h}, \\
&+ \frac{\rho_{b,c}}{6\sqrt{3\theta_{b,h}}}[([M - V_b - \sqrt{3\theta_{b,h}}]^2 \\
&- [M - \sqrt{3\theta_{c,h}}]^2)^{3/2} - ([M - V_b + \sqrt{3\theta_{b,h}}]^2 \\
&- [M - \sqrt{3\theta_{c,h}}]^2)^{3/2}],
\end{aligned} \tag{29}$$

and the following equation for the upper limit in M in the case of *co-propagating* ($V_b > 0$),

$$\begin{aligned}
F_2(M) = &\ -\frac{1}{2}(1 + \rho_{h,c} + \rho_{b,c})(M - V_b - \sqrt{3\theta_{b,h}})^2 \\
&+ M^2 + \theta_{c,h} + \rho_{b,c}\theta_{b,h} + \rho_{b,c}(M - V_b)^2 \\
&- \frac{4}{3}\rho_{b,c}(M - V_b)^{3/2}(3\theta_{b,h})^{1/4}. \\
&+ \rho_{h,c}\left[1 - \left(1 + \frac{[M - V_b - \sqrt{3\theta_{b,h}}]^2}{2\kappa - 3}\right)^{-\kappa + 3/2}\right] \\
&+ \frac{1}{6\sqrt{3\theta_{c,h}}}[([M - \sqrt{3\theta_{c,h}}]^2 \\
&- [M - V_b - \sqrt{3\theta_{b,h}}]^2)^{3/2} - ([M + \sqrt{3\theta_{c,h}}]^2 \\
&- [M - V_b - \sqrt{3\theta_{b,h}}]^2)^{3/2}].
\end{aligned} \tag{30}$$

Solving equations (29) and (30) constrains the upper limit for the Mach number, $M_2(\kappa$, $\rho_{h,c}$, $\theta_{c,h}$, $\rho_{b,c}$, $\theta_{b,h}$, V_b). In the absence of the electron beam, equations (28) and (29) recover precisely equations (34) and (36) in [42].

The soliton existence regions are shown in figures 2–4 for different parameters of the electron beam and different values of the suprathermality (described by κ) of the hot electrons. Solitary structures of the electrostatic potential may occur in the range $M_1 < M < M_2$, which depends on the parameters κ, $\rho_{h,c}$, $\theta_{c,h}$, $\rho_{b,c}$, $\theta_{b,h}$ and V_b. Furthermore, we assumed that the cool electrons are supersonic ($M > \sqrt{3\theta_{c,h}}$), as well as the electron beam
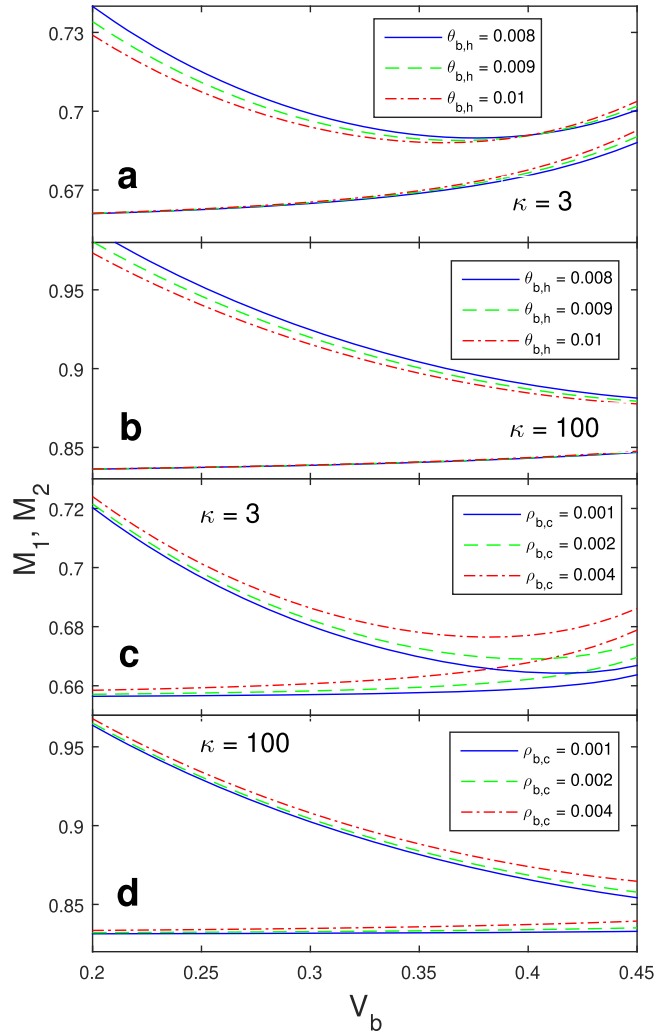
Figure 2. Variation of the lower limit for the Mach number M_1 (lower curves) and the upper limit for the Mach number M_2 (upper curves) with the positive normalized beam speed V_b for different values of the beam-to-hot electron temperature ratio $\theta_{b,h}$ (a)–(b) and different values of the beam-to-cool electron number density ratio $\rho_{b,c}$ (c)–(d). Solitons may exist for values of the Mach number M in the region between the lower and the upper curve(s) of the same style/color. (a)–(b) Curves: $\theta_{b,h} = 0.008$ (solid), 0.009 (dashed), and 0.01 (dotted–dashed). Here, we have taken: (a) $\kappa = 3$ and (b) $\kappa = 100$. (c)–(d) Curves: $\rho_{b,c} = 0.001$ (solid), 0.002 (dashed), and 0.004 (dotted–dashed). Here, we have taken: (c) $\kappa = 3$ and (d) $\kappa = 100$. The remaining parameters are $\rho_{h,c} = 1.5$, $\rho_{b,c} = 0.008$ and $\theta_{c,h} = \theta_{b,h} = 0.01$, unless values are specified.
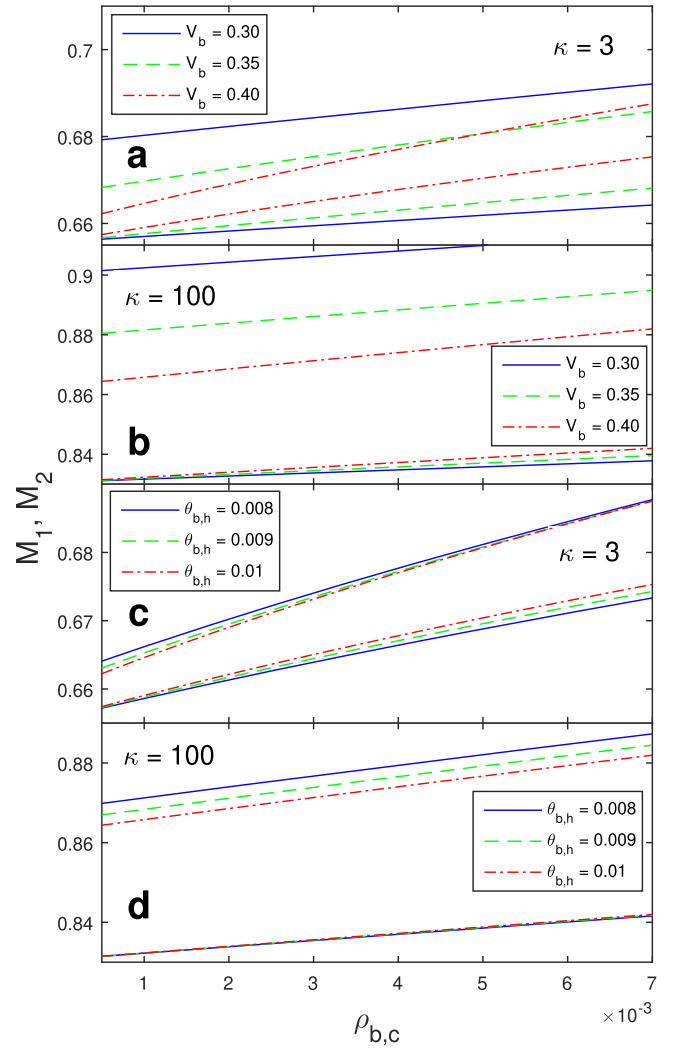
Figure 3. Variation of the lower limit for the Mach number M_1 (lower curves) and the upper limit for the Mach number M_2 (upper curves) with the beam-to-cool electron number density ratio $\rho_{b,c}$ for different values of the positive normalized beam speed V_b (a)–(b) an0ature ratio $\theta_{b,h}$ (c)–(d). Solitons may exist for values of the Mach number M in the region between the lower and the upper curve(s) of the same style/color. (a)–(b) Curves: $V_b = 0.3$ (solid), 0.35 (dashed), and 0.4 (dotted–dashed). Here, we have taken: (a) $\kappa = 3$ and (b) $\kappa = 100$. (c)–(d) Curves: $\theta_{b,h} = 0.008$ (solid), 0.009 (dashed), and 0.01 (dotted–dashed). Here, we have taken: (c) $\kappa = 3$ and (d) $\kappa = 100$. The remaining parameters are $\rho_{h,c} = 1.5$, $V_b = 0.4$ and $\theta_{c,h} = \theta_{b,h} = 0.01$, unless values are specified.

$M > V_b + \sqrt{3\theta_{b,h}}$), whereas the hot electrons are subsonic ($M < 1$).

Figure 2 shows the existence domain of EAWs in two opposite cases: in (a) a very high suprathermality ($\kappa = 3$), and (b) a very low suprathermality ($\kappa = 100$). The normalized beam speed is positive ($V_b > 0$), which means that the soliton *co-propagates* with the electron beam. We see that the existence domain of the Mach number becomes narrower with strong suprathermality and higher values of the normalized beam speed. Comparing the two frames (a) and (b), or (c) and (d) in figure 2, we notice that low values of κ impose that the soliton propagates at lower Mach number

range. From figures 2(a)–(b), it can be seen that increasing the electron beam thermal pressure ($\theta_{b,h}$) shrinks the soliton existence region. Finally, we note that lower values of the beam-to-cool electron number density ratio ($\rho_{b,c}$; also see figure 3 for this effect) shrink the permitted soliton region, nearly down to nil, for very high V_b ($\geqslant 0.5$) and strong suprathermality (low κ).

As seen in figures 2 and 3, the existence region becomes narrower for lower values of $\rho_{b,c}$ and κ. This is especially visible in figures 2(a), (c); an increase in $\rho_{b,c}$ broadens the permitted region of the Mach number. It is in contrast to increasing the hot-to-cool electron number density ratio ($\rho_{h,c}$),
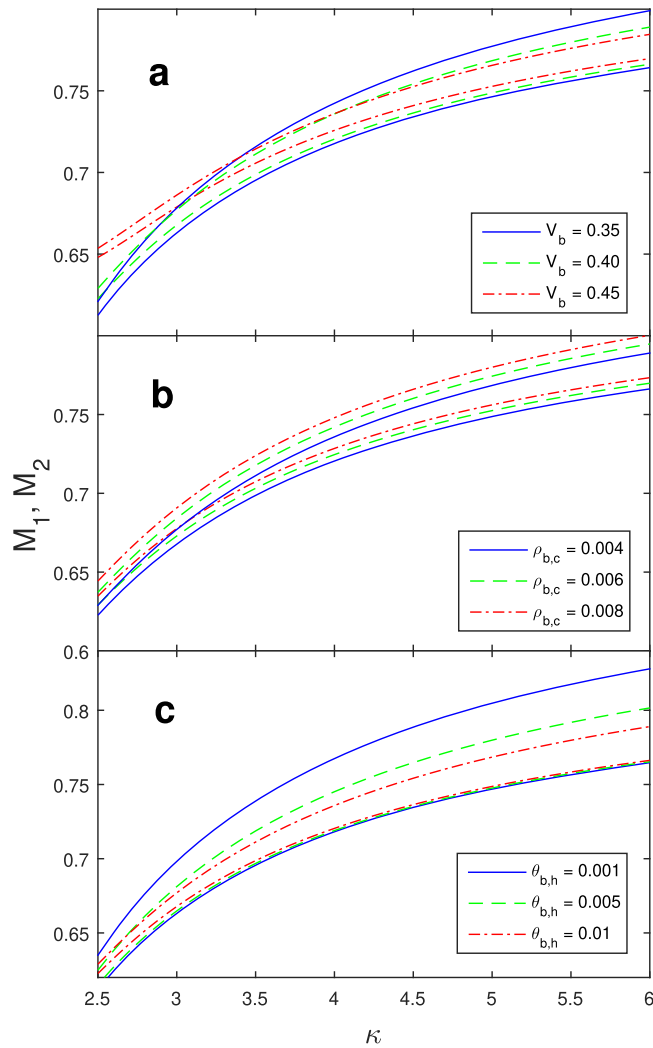
Figure 4. Variation of the lower limit for the Mach number M_1 (lower curves) and the upper limit for the Mach number M_2 (upper curves) with the suprathermality parameter κ for different values of the positive normalized beam speed V_b (upper panel), the beam-to-cool electron number density ratio $\rho_{b,c}$ (middle panel) and the beam-to-hot electron temperature ratio $\theta_{b,h}$ (bottom panel). Solitons may exist for values of the Mach number M in the region between the lower and upper curves of the same style/color. Upper panel: $V_b = 0.35$ (solid curve), 0.40 (dashed), and 0.45 (dotted–dashed). Here, we have taken $\rho_{h,c} = 1.5$, $\theta_{c,h} = \theta_{b,h} = 0.01$ and $\rho_{b,c} = 0.004$. Middle panel: $\rho_{b,c} = 0.004$ (solid curve), 0.006 (dashed), and 0.008 (dotted–dashed). Here, we have taken $\rho_{h,c} = 1.5$, $\theta_{c,h} = \theta_{b,h} = 0.01$ and $V_b = 0.4$. Lower panel: $\theta_{b,h} = 0.001$ (solid curve), 0.005 (dashed), and 0.01 (dotted–dashed). Here, we have taken $\rho_{h,c} = 1.5$, $\rho_{b,c} = 0.004$, $\theta_{c,h} = 0.01$ and $V_b = 0.4$.

which shrinks down the existence region [42]. We know that a reduction in the cool electron density (increasing $\rho_{h,c}$) was responsible for shrinking the existence region. Moreover, we also notice that a reduction in the electron beam density (decreasing $\rho_{b,c}$) has a similar effect in the soliton existence region. Similarly, figure 3 (also see figure 2) shows that higher values of the normalized beam speed V_b and the temperature ratio $\theta_{b,h}$ shrink the permitted region in a strong suprathermality (low κ).

Figure 4 demonstrates the effect of the hot electron κ-distribution. The acoustic limits (M_1 and M_2) decrease rapidly as approaching the limiting value $\kappa \to 3/2$. Moving toward a Maxwellian distribution ($\kappa \to \infty$) broadens the permitted range of the Mach number. The result is similar to the trend in figures 2 and 3; stronger suprathermality imposes that solitons occur in compressed ranges of the Mach number. It is quite similar to what we found in our previous model without the electron beam [42].

We also notice that varying the negative normalized beam speed ($V_b < 0$) trivially change the lower limit M_1 and the upper limit M_2 under the excitation conditions $\rho_{b,c} V_b \ll 1$ and $\theta_{b,h} \ll 0.1$ (figures not shown here). Similarly, the electron beam thermal pressure ($\theta_{b,h}$) and the beam-to-cool electron number density ratio ($\rho_{b,c}$) have trivial effects on the existence domain (not shown here) when the normalized beam speed is negative, in contrast to what we saw in figures 2(a), (b). Therefore, the existence domain of EAWs does not affect largely when the soliton *counter-propagates* with the electron beam.

6. Nonlinear electron-acoustic wave structures

To study the localized structures of large-amplitude EAWs, we have solved equation (26) via numerical integration for various plasma parameters, which allow us to observe their effects on the nonlinear wave structures. We have found only negatively polarized solitons, in contrast to what found in [23], as the κ-distribution may not facilitate reverse polarity of electrostatic solitary waves. To have positive polarity in our fluid model, a mobile positive charge such as ion and positron is required to support the inertia for acoustic oscillations, while the suprathermal hot electrons provide the wave restoring force. However, the ion inertia propagates electrostatic waves in a slow-acoustic mode [54]. Thus, mobile positrons (or electron holes) may provide the inertia to have positive polarity in a fast-acoustic mode similar to the negatively polarized electron-acoustic solitons [58].

Figure 5 shows the variation of the pseudopotential $\Psi(\phi)$ with the normalized potential ϕ, for different values of the positive normalized beam speed V_b (keeping $\rho_{h,c} = 1$, $\rho_{b,c} = 0.008$, $\theta_{c,h} = \theta_{b,h} = 0.01$, $\kappa = 4.0$ and Mach number $M = 0.9$, all fixed). The pulse amplitude $|\phi_m|$ decreases with increasing V_b, which are in agreement with [30, 31, 49]. We algebraically determined the fluid density (figure 5(c)) and velocity disturbances (figure 5(d)) of the cool electrons and the electron beam (figures 5(e), (f)). It is noticeable that an increase in positive V_b (co-propagation) compresses the disturbances of u_c, n_c, n_b and $u_b - V_b$. Similarly, figure 6 depicts the variation of the pseudopotential $\Psi(\phi)$ for different values of the negative normalized beam speed V_b. It is seen that the pulse amplitude $|\phi_m|$ is slightly altered with a change in negative V_b (counter-propagation), in contrast to what we saw in figure 5.
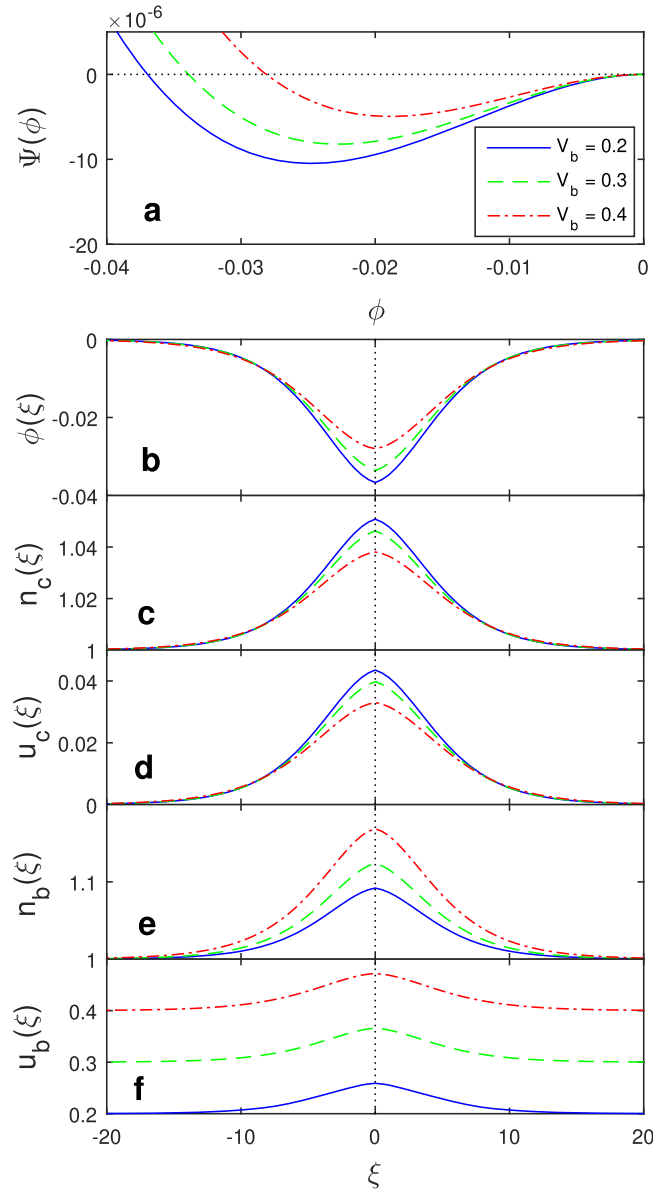
Figure 5. (a) The pseudopotential $\Psi(\phi)$ of electron-acoustic solitons and the associated solutions: (b) electric potential pulse ϕ, (c) density n and (d) velocity u of the cool electron fluid, (e) density n_b and (f) velocity u_b of the electron beam are depicted versus position ξ, for different values of the positive normalized beam speed V_b. We have taken: $V_b = 0.2$ (solid curve), 0.3 (dashed curve), and 0.4 (dotted–dashed curve). The other parameter values are: $\rho_{h,c} = 1$, $\rho_{b,c} = 0.008$, $\theta_{c,h} = \theta_{b,h} = 0.01$, $\kappa = 4.0$ and $M = 0.9$.

Figure 7 shows the variation of the pseudopotential $\Psi(\phi)$ for different values of the beam-to-cool electron number density ratio $\rho_{b,c}$. Both the root and the depth of the Sagdeev potential well increase with decreasing $\rho_{b,c} = n_{b,0}/n_{c,0}$. This means that increasing the cool electron density and/or decreasing the electron beam density increases the negative polarity solitary waves.

Figure 8 shows the thermal effect of the electron beam through $\theta_{b,h} = T_b/T_h$, which agrees with [30, 49]. We see that the soliton excitations are amplified with either an increase in the suprathermal hot electron temperature (T_h) or a decrease
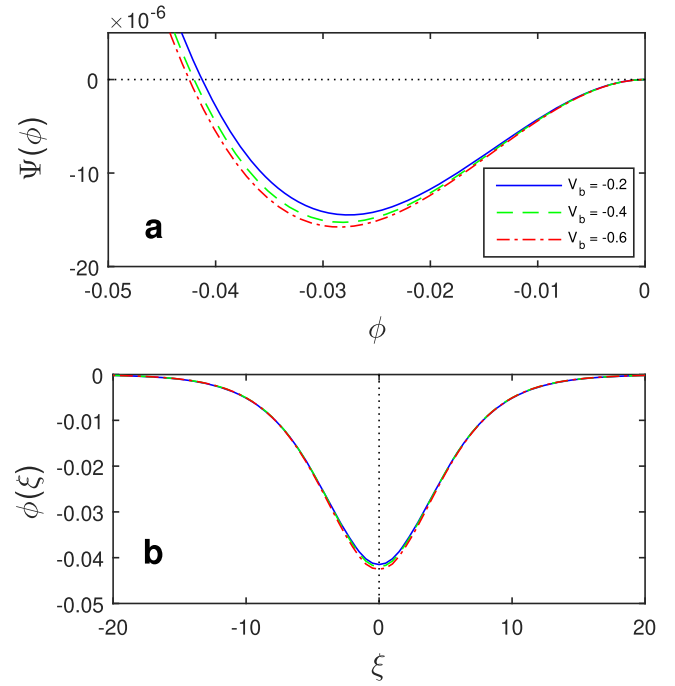

Figure 6. (a) The pseudopotential $\Psi(\phi)$ of electron-acoustic solitons and the associated solutions: (b) electric potential pulse ϕ is depicted versus position ξ, for different values of the negative normalized beam speed V_b. We have taken: $V_b = -0.2$ (solid curve), -0.4 (dashed curve), and -0.6 (dotted–dashed curve). The other parameter values are: $\rho_{h,c} = 1$, $\rho_{b,c} = 0.008$, $\theta_{c,h} = \theta_{b,h} = 0.01$, $\kappa = 4.0$ and $M = 0.9$.
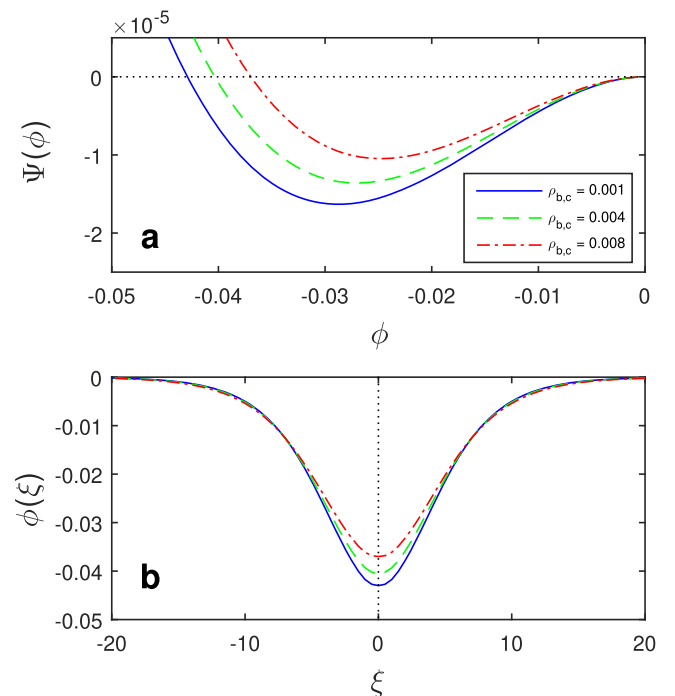

Figure 7. (a) The pseudopotential $\Psi(\phi)$ of electron-acoustic solitons and the associated solutions: (b) electric potential pulse ϕ is depicted versus position ξ, for different values of the beam-to-cool electron number density ratio $\rho_{b,c}$. From bottom to top: $\rho_{b,c} = 0.001$ (solid curve); 0.004 (dashed curve); 0.008 (dotted–dashed curve). Here $\rho_{h,c} = 1$, $\theta_{c,h} = \theta_{b,h} = 0.01$, $V_b = 0.2$, $\kappa = 4.0$ and $M = 0.9$.
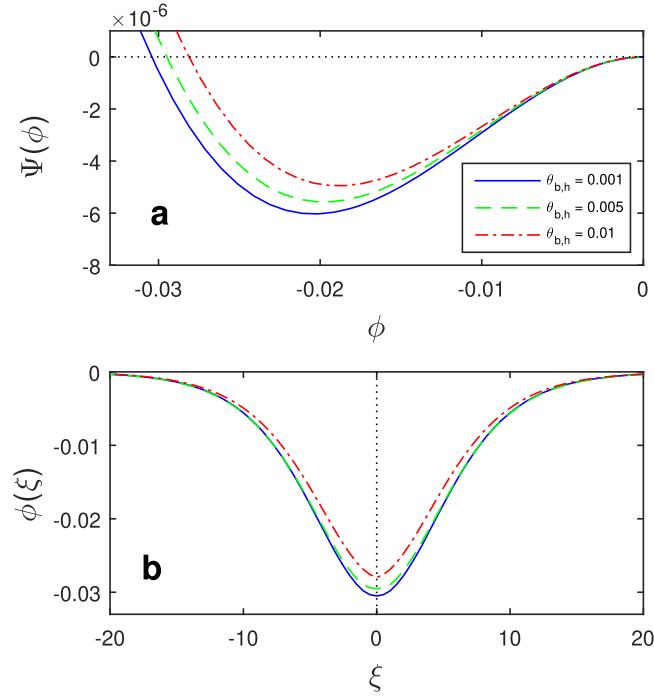
Figure 8. (a) The pseudopotential $\Psi(\phi)$ of electron-acoustic solitons and the associated solutions: (b) electric potential pulse ϕ is depicted versus position ξ, for different values of the beam-to-hot electron temperature ratio $\theta_{b,h}$. From bottom to top: $\theta_{b,h} = 0.001$ (solid curve); 0.005 (dashed curve); 0.01 (dotted–dashed curve). Here $\rho_{h,c} = 1$, $\rho_{b,c} = 0.008$, $\theta_{c,h} = 0.01$, $V_b = 0.4$, $\kappa = 4.0$ and $M = 0.9$.

in the electron beam temperature (T_b). Therefore, thermal effects of the hot electrons relative to the electron beam amplify the electric potential at a fixed Mach number (similar to what found for the hot relative to the cool electrons via $\theta_{c,h} = T_c/T_h$ in [42]).

Figure 9 summarizes the behavior of the negative polarity EAWs co-propagating with the beam speed ($V_b > 0$). It can be seen that the maximum absolute pulse amplitude $|\phi_m|$ of negative electric potentials is significantly reduced by increasing the normalized beam speed V_b and the beam-to-cool electron number density ratio $\rho_{b,c}$ (see figures 9(a), (b)). However, an increase in the beam-to-hot electron temperature ratio $\theta_{b,h}$ slightly decreases the maximum absolute pulse amplitude $|\phi_m|$ of negative electric potentials (see figure 9(c)). Similarly, in figure 10, we have depicted the variation of the absolute pulse amplitude of negative polarity EAWs counter-propagating with the electron beam ($V_b < 0$) versus the normalized beam speed V_b and the beam-to-cool electron number density ratio $\rho_{b,c}$. It is seen that the absolute pulse amplitude $|\phi_m|$ of negatively polarized EAWs slightly grows with an increase in the absolute normalized speed $|V_b|$ of the counter-propagating electron beam. Moreover, figure 10(b) shows that the absolute pulse amplitude of negative polarity solitons is slightly reduced by increasing the beam-to-cool electron number density ratio $\rho_{b,c}$ in the counter-propagation case,
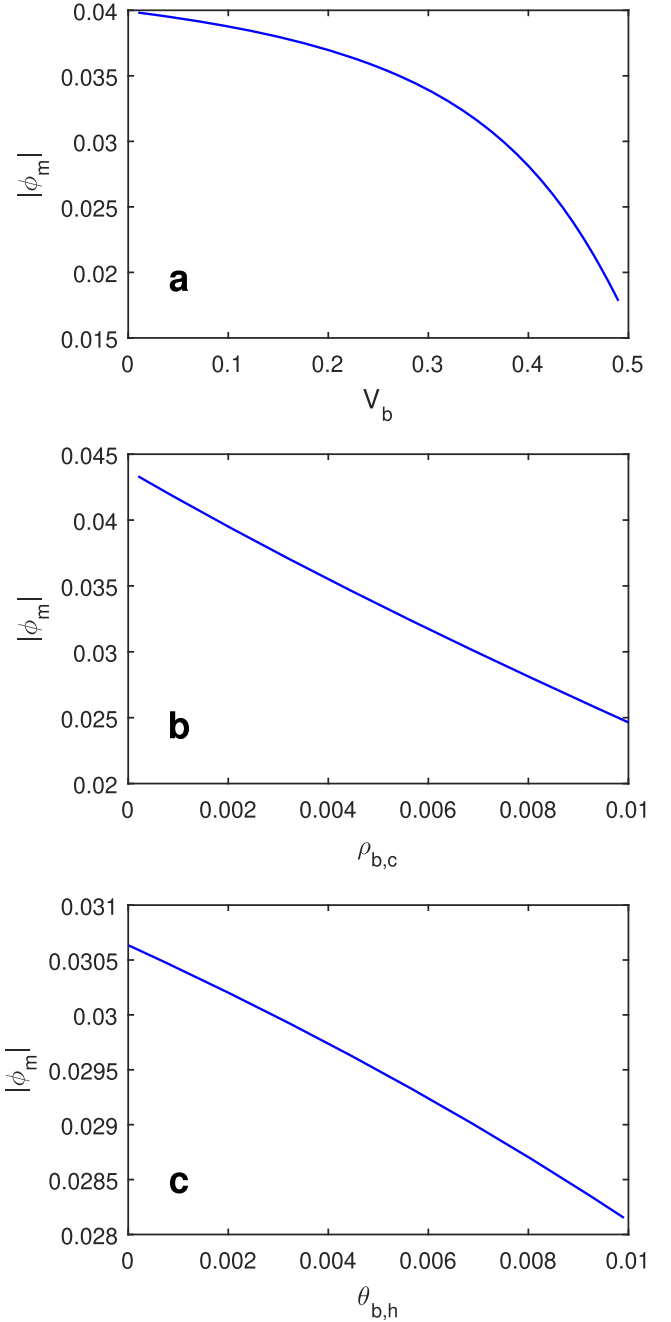

Figure 9. Variation of the absolute pulse amplitude $|\phi_m|$ of electron-acoustic solitons versus (a) the positive normalized beam speed V_b, (b) the beam-to-cool electron number density ratio $\rho_{b,c}$, and (c) the beam-to-hot electron temperature ratio $\theta_{b,h}$. The remaining parameters are $\rho_{h,c} = 1$, $\rho_{b,c} = 0.008$, $\theta_{c,h} = 0.01$, $\theta_{b,h} = 0.01$, $V_b = 0.4$, $\kappa = 4.0$ and $M = 0.9$, unless values are specified.

which is dissimilar to the large amplification in the co-propagation case shown in figure 9(b). Under the trivially current ($\rho_{b,c}V_b \ll 1$) and weakly damped ($\theta_{b,h} \ll 0.1$) excitation conditions, varying the beam-to-hot electron temperature ratio $\theta_{b,h}$ insignificantly alters the maximum absolute pulse amplitude of negative electric potentials in the counter-propagation situation (figure not presented here).
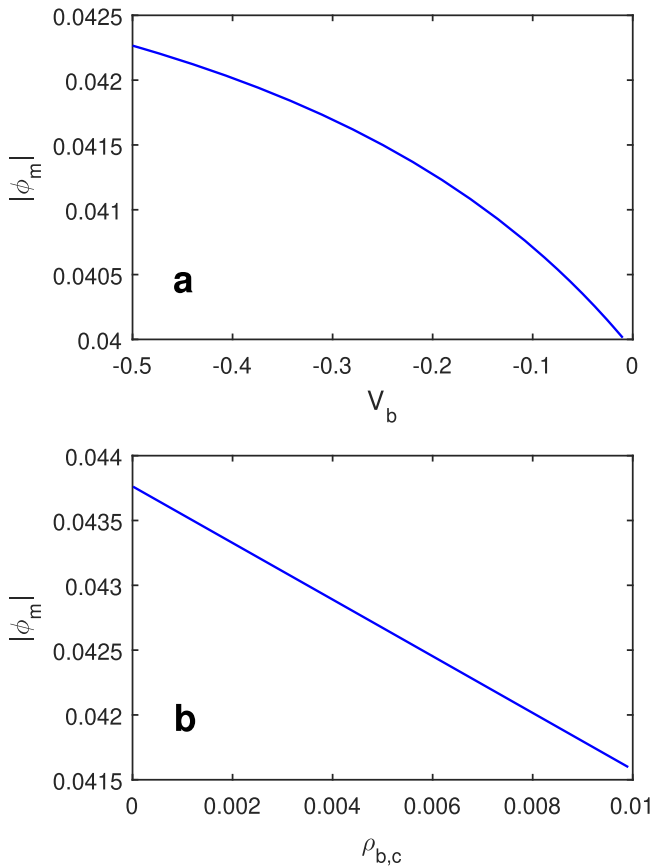
Figure 10. Variation of the absolute pulse amplitude $|\phi_m|$ of electron-acoustic solitons versus (a) the negative normalized beam speed V_b and (b) the beam-to-cool electron number density ratio $\rho_{b,c}$. The remaining parameters are $\rho_{h,c} = 1$, $\rho_{b,c} = 0.008$, $\theta_{c,h} = 0.01$, $\theta_{b,h} = 0.01$, $V_b = -0.4$, $\kappa = 4.0$ and $M = 0.9$, unless values are specified.

7. Conclusions

We have studied the propagation of EAWs in a collisionless, unmagnetized plasma model consisting of cool inertial background electrons, cool inertial beam electrons, κ-distributed suprathermal hot electrons and stationary ions.

We have obtained a linear dispersion relation for the small-amplitude EAWs and determined the effects of electron beam properties on the dispersion relation, through the beam-to-cool electron population ratio $\rho_{b,c}$ and the normalized beam speed V_b. It is found that the phase speed increases weakly with an increase in $\rho_{b,c}$ and V_b, while it is largely decreased by increasing the suprathermality (decreasing κ and increasing $\rho_{h,c}$; see [42]).

We have employed the Sagdeev's pseudopotential technique to study the nonlinear dynamics of large-amplitude EAWs, and to determine the permitted parametric regions where allow solitons to propagate in the plasma. The results of this study indicate that the existence domain of solitons, which *co-propagate* with the electron beam ($V_b > 0$), becomes narrower with an increase in the suprathermality (decreasing the spectral index κ), increasing the normalized beam speed V_b, decreasing the beam-to-cool electron

population ratio $\rho_{b,c}$, and increasing the beam-to-hot electron temperature ratio $\theta_{b,h}$. However, the *counter-propagation* ($V_b < 0$) slightly affects the existence domain of the nonlinear EAWs.

We have numerically solved the pseudo-energy balance equation (26) to study effects of various plasma parameters on the nonlinear EAWs. It is found that increasing the beam-to-cool electron density ratio $\rho_{b,c}$ largely decreases the electric potential amplitude in the co-propagation case ($V_b > 0$; see figures 7 and 9), but slightly in the counter-propagation case ($V_b < 0$; see figure 10). Increasing the positive beam speed ($V_b > 0$) significantly decreases the soliton electric potential amplitude (figures 5 and 9). However, a change in the negative beam speed ($V_b < 0$) slightly alters the electric potential amplitude (figures 6 and 10) under the excitation conditions ($\rho_{b,c} V_b \ll 1$ and $\theta_{b,h} \ll 0.1$). We also see that decreasing the beam-to-hot electron temperature ratio $\theta_{b,h}$ slightly amplifies the electric potential amplitude in the co-propagation case ($V_b > 0$; see figures 8 and 9), but insignificantly alters the soliton pulse in the counter-propagation situation ($V_b < 0$) under the excitation conditions. Some of these results are aligned with the previous findings by other authors [30, 31, 49].

Our two-fluid model predicts only the propagation of negatively polarized EAWs. However, we did not find any positive polarity electrostatic solitons. This is in agreement with [30], but disagrees with [23, 31]. Apparently, the inclusion of κ-distribution (or inertialess) electrons does not permit positive polarity electrostatic solitons. References [52, 61] concluded that positive polarity electrostatic solitary waves can be produced in a parameter range if hot electron inertia is retained. In order to find solitons with a positive polarity signature, it is imperative to retain hot electron inertia in combination with the thermal effects [53]. However, it still requires a high density of cool electrons to produce positive electrostatic potential solitons [53], larger than what are currently measured in observations. It is known that the ion inertia, combined with suprathermal electrons, can generate positive polarity electrostatic waves, but in the ion-acoustic mode, and propagate much slower than electrostatic solitary waves in the electron-acoustic mode (see e.g. [54]). Alternatively, mobile cool positrons (or electron holes), together with suprathermal hot electrons, may support positive polarity electrostatic waves with the propagation speed comparable to the negative polarity electron-acoustic solitons [58].

The present study was motivated by electrostatic solitary waves observed in the BEN [17], the PCBL region [20], the magnetopause [21], and the magnetosheath [22] of the Earth's magnetosphere, where hot suprathermal electrons and magnetic field-aligned electron beams are found to be present. For example, considering the parameters of the BEN plasma ($T_b \sim 1$ eV [59], $T_h \sim 990$ eV, and $n_c \sim n_h \sim 10$ cm^{-3} [17]), the peak-to-peak amplitude of the normalized electric field is calculated to be $E = -\partial\phi/\partial x \approx 7 \times 10^{-3}$ (figures not shown) based on the electric potential pulse ϕ at $\theta_{b,h} = T_b/T_h = 0.001$ with the physical parameters listed in figure 8. This corresponds to a peak-to-peak electric field of $E \approx 90$ mV m^{-1} (potential ϕ and space x are,

respectively, unnormalized by $k_B T_h/e = 9.9 \times 10^5$ mV and $\lambda_0 = \sqrt{\varepsilon_0 k_B T_h/n_{c,0}e^2} = 74$ m), which is in agreement with the peak-to-peak electric filed of ~ 100 mV m^{-1} observed in the BEN [17]. Similarly, the parameters of the magnetosphere plasma observed by the MMS mission [21, 22] ($T_b \sim 1$ eV, $T_h \sim 1$ keV, $n_b \sim 0.2$ cm^{-3}, and $n_h \sim 30$ cm^{-3}) yield a peak-to-peak electric field of $E \approx 160$ mV m^{-1} ($k_B T_h/e = 10^6$ mV and $\lambda_0 = 43$ m), which is roughly close to the large-amplitude, parallel electric fields of ~ 100 mV m^{-1} measured at the magnetic reconnection region of the Earth's magnetopause [21].

In conclusion, the parametric investigations presented in sections 5 and 6 suggest that the propagation of EAWs, as well as the nonlinear dynamics of large-amplitude electrostatic wave structures, can be altered by the electron beam, in the presence of suprathermal electrons. The results could have important implications for the characteristics of nonlinear plasma waves observed in several space and astrophysical plasma environments such as the Earth's magnetosphere.

Acknowledgments

ORCID iDs

A Danehkar ● https://orcid.org/0000-0003-4552-5997

References

[1] Watanabe K and Taniuti T 1977 *J. Phys. Soc. Japan* **43** 1819
[2] Ikezawa S and Nakamura Y 1981 *J. Phys. Soc. Japan* **50** 962–7
[3] Mace R L and Hellberg M A 1990 *J. Plasma Phys.* **43** 239–55
[4] Hellberg M A, Mace R L, Armstrong R J and Karlstad G 2000 *J. Plasma Phys.* **64** 433–43
[5] Dubouloz N, Pottelette R, Malingre M and Treumann R A 1991 *Geophys. Res. Lett.* **18** 155–8
[6] Feldman W C, Anderson R C, Bame S J, Gary S P, Gosling J T, McComas D J, Thomsen M F, Paschmann G and Hoppe M M 1983 *J. Geophys. Res.* **88** 96–110
[7] Bale S D, Kellogg P J, Larsen D E, Lin R P, Goetz K and Lepping R P 1998 *Geophys. Res. Lett.* **25** 2929–32
[8] Pottelette R, Ergun R E, Treumann R A, Berthomier M, Carlson C W, McFadden J P and Roth I 1999 *Geophys. Res. Lett.* **26** 2629–32
[9] Cattell C, Crumley J, Dombeck J, Wygant J R and Mozer F S 2002 *Geophys. Res. Lett.* **29** 1065
[10] Baluku T K, Hellberg M A and Mace R L 2011 *J. Geophys. Res. (Space Phys.)* **116** A04227
[11] Gary S P and Tokar R L 1985 *Phys. Fluids* **28** 2439–41

[12] Mace R L, Amery G and Hellberg M A 1999 *Phys. Plasmas* **6** 44–9
[13] Tokar R L and Gary S P 1984 *Geophys. Res. Lett.* **11** 1180–3
[14] Lin C S, Burch J L, Shawhan S D and Gurnett D A 1984 *J. Geophys. Res.* **89** 925–35
[15] Ogilvie K W, Fitzenreiter R J and Scudder J D 1984 *J. Geophys. Res.* **89** 10723–32
[16] Pottelette R, Malingre M, Dubouloz N, Aparicio B and Lundin R 1990 *J. Geophys. Res.* **95** 5957–71
[17] Dubouloz N, Pottelette R, Malingre M, Holmgren G and Lindqvist P A 1991 *J. Geophys. Res.* **96** 3565–79
[18] Matsumoto H, Kojima H, Miyatake T, Omura Y, Okada M, Nagano I and Tsutsui M 1994 *Geophys. Res. Lett.* **21** 2915–8
[19] Cattell C, Wygant J, Dombeck J, Mozer F S, Temerin M and Russell C T 1998 *Geophys. Res. Lett.* **25** 857–60
[20] Tsurutani B T, Arballo J K, Lakhina G S, Ho C M, Buti B, Pickett J S and Gurnett D A 1998 *Geophys. Res. Lett.* **25** 4117–20
[21] Ergun R E *et al* 2016 *Geophys. Res. Lett.* **43** 5626–34
[22] Holmes J C, Ergun R E, Newman D L, Wilder F D, Sturner A P, Goodrich K A, Torbert R B, Giles B L, Strangeway R J and Burch J L 2018 *J. Geophys. Res. (Space Phys.)* **123** 132–45
[23] Berthomier M, Pottelette R, Malingre M and Khotyaintsev Y 2000 *Phys. Plasmas* **7** 2987–94
[24] Mace R L and Hellberg M A 2001 *Phys. Plasmas* **8** 2649–56
[25] Sahu B and Roychoudhury R 2004 *Phys. Plasmas* **11** 1947–54
[26] El-Taibany W F 2005 *J. Geophys. Res. (Space Phys.)* **110** A01213
[27] El-Taibany W F and Moslem W M 2005 *Phys. Plasmas* **12** 032307
[28] El-Labany S K, El-Taibany W F and El-Abbasy O M 2005 *Phys. Plasmas* **12** 092304
[29] Elwakil S A, Zahran M A and El-Shewy E K 2007 *Phys. Scr.* **75** 803–8
[30] Devanandhan S, Singh S V, Lakhina G S and Bharuthram R 2011 *Nonlinear Process. Geophys.* **18** 627–34
[31] Singh S V, Lakhina G S, Bharuthram R and Pillay S R 2011 *Phys. Plasmas* **18** 122306
[32] Lakhina G S, Singh S V, Kakad A P, Verheest F and Bharuthram R 2008 *Nonlinear Process. Geophys.* **15** 903–13
[33] Lakhina G S, Singh S V and Kakad A P 2011 *Adv. Space Res.* **47** 1558–67
[34] Gosling J T, Thomsen M F, Bame S J and Russell C T 1989 *J. Geophys. Res.* **94** 10011–25
[35] Pierrard V and Lazar M 2010 *Sol. Phys.* **267** 153–74
[36] Vasyliunas V M 1968 *J. Geophys. Res.* **73** 2839–84
[37] Summers D and Thorne R M 1991 *Phys. Fluids* B **3** 1835–47
[38] Baluku T K and Hellberg M A 2008 *Phys. Plasmas* **15** 123705
[39] Hellberg M A, Mace R L, Baluku T K, Kourakis I and Saini N S 2009 *Phys. Plasmas* **16** 094701
[40] Sahu B 2010 *Phys. Plasmas* **17** 122305
[41] Younsi S and Tribeche M 2010 *Astrophys. Space Sci.* **330** 295–300
[42] Danehkar A, Saini N S, Hellberg M A and Kourakis I 2011 *Phys. Plasmas* **18** 072902
[43] Devanandhan S, Singh S V and Lakhina G S 2011 *Phys. Scr.* **84** 025507
[44] Sultana S and Kourakis I 2012 *Eur. Phys. J.* D **66** 100
[45] Sultana S, Kourakis I and Hellberg M A 2012 *Plasma Phys. Control. Fusion* **54** 105016
[46] Sahu B 2013 *Europhys. Lett.* **101** 55002
[47] Han J N, Duan W S, Li J X, He Y L, Luo J H, Nan Y G, Han Z H and Dong G X 2014 *Phys. Plasmas* **21** 012102
[48] Han J N, Duan W S, Li J X, Dong G X and Ge S H 2014 *Astrophys. Space Sci.* **351** 525–31

[49] Singh S V, Devanandhan S, Lakhina G S and Bharuthram R 2016 *Phys. Plasmas* **23** 082310

[50] Danehkar A, Saini N S, Hellberg M A and Kourakis I 2011 *AIP Conf. Proc.* **1397** 305–6

[51] Danehkar A, Kourakis I and Hellberg M A 2014 *IEEE 41st International Conference on Plasma Sciences (ICOPS), High-Power Particle Beams (BEAMS)* p 7012747

[52] Verheest F, Cattaert T and Hellberg M A 2005 *Space Sci. Rev.* **121** 299–311

[53] Verheest F, Hellberg M A and Lakhina G S 2007 *Astrophys. Space Sci. Trans.* **3** 15–20

[54] Danehkar A 2009 *Master's Thesis* Queen's University Belfast, Northern Ireland, UK doi:10.5281/zenodo.47796

[55] Saini N S and Kourakis I 2010 *Plasma Phys. Control. Fusion* **52** 075009

[56] Saberian E, Esfandyari-Kalejahi A, Rastkar-Ebrahimzadeh A and Afsari-Ghazi M 2013 *Phys. Plasmas* **20** 032307

[57] Jilani K, Mirza A M and Khan T A 2014 *Astrophys. Space Sci.* **349** 255–63

[58] Danehkar A 2017 *Phys. Plasmas* **24** 102905

[59] Schriver D and Ashour-Abdalla M 1989 *Geophys. Res. Lett.* **16** 899–902

[60] Verheest F 2009 *J. Phys. A: Math. Theor.* **42** 285501

[61] Cattaert T, Verheest F and Hellberg M A 2005 *Phys. Plasmas* **12** 042901